



Mechanisms of Oxygen Precipitation in Cz-Si Wafers Subjected to Rapid Thermal Anneals

Andrey Sarikov,^{a,z} Vladimir Litovchenko,^{a,*} Igor Lisovskyy,^a Maria Voitovich,^a Sergei Zlobin,^a Vasyi Kladko,^a Nikolay Slobodyan,^a Vladimir Machulin,^a and Cor Claeys^{b,c,**}

^aV. Lashkarev Institute of Semiconductor Physics, National Academy of Sciences of Ukraine, 03028 Kiev, Ukraine

^bimec, Kapeldreef 75, 3001 Leuven, Belgium

^cE.E. Dept. K.U.Leuven, Kasteelpark Arenberg 10, 3001 Leuven, Belgium

The mechanisms of oxygen precipitation in the SiO₂ phase during rapid thermal annealing of solar-grade Cz-Si wafers at moderate temperature (850 °C) are analysed. A theoretical model is derived to study the kinetics of oxygen precipitate growth that takes into account a significant increase in the non-equilibrium solubility of oxygen and the increased effective diffusivity of oxygen atoms. A mechanism for the mentioned abnormal modifications of the characteristics of oxygen diffusivity and solubility is suggested based on the dominating influence of excess point defects appearing in the Si wafers during the rapid thermal anneals.

© 2011 The Electrochemical Society. [DOI: 10.1149/1.3594724] All rights reserved.

Manuscript submitted January 28, 2011; revised manuscript received April 18, 2011. Published June 7, 2011.

In the crystalline Si technology, the use of high temperature (~1200 °C and above) rapid thermal anneals (RTAs) has become an efficient tool to dissociate silicon oxide precipitates and to restore the supersaturated solution of oxygen in silicon.^{1–3} The introduction of excess vacancies during such treatments allows to transfer in a controlled manner this supersaturated solution back into SiO₂ precipitates during subsequent furnace anneals. This process is the so called Magic Denude Zone concept.⁴ Vacancies are known to promote the formation of silicon oxide precipitates in Si by the release of strain caused by the volume mismatch between the Si and the SiO₂ phase substructures.⁵

A number of publications has been devoted to the study of the effect of a RTA pre-treatment on the oxygen precipitation kinetics as a result of subsequent high temperature (~1000–1100 °C) thermal anneals in a furnace.^{1,6–10} Oxygen precipitation is enhanced by raising the temperature and the duration of the short time RTA pre-treatment. A crucial role is also played by the RTA atmosphere. It is well-known that rapid thermal anneals in a nitrogen atmosphere lead to an excess of silicon vacancies due to the Si surface nitridation effect^{6,9} and therefore to an enhanced oxygen precipitation process. On the other hand, RTA in an oxygen atmosphere leads to precipitation retardation, which is a result of the introduction of excess Si self-interstitials generated by surface oxidation.¹

Most of the earlier studies related to the influence of RTA on oxygen precipitation in Si wafers concerned the precipitation during conventional furnace anneals *after* RTA pre-treatments. We have found, recently, that the rapid thermal anneals of solar grade Czochralski-grown Si(Cz-Si) wafers at moderate (~850 °C) temperatures in air causes *itself* an accelerated oxygen precipitation with the formation of a silicon oxide phase consisting of SiO₄ tetrahedra with a 4- and 6-member ring structure as well as Si₂O₂Si_{4–y} molecular complexes. In contrast, in microelectronic grade Si mostly weakly strained SiO₂ precipitates consisting of mainly 6-member rings of SiO₄ tetrahedra are formed.¹⁰ In this work, a detailed theoretical analysis is made of the enhanced formation of SiO₂ precipitates in solar grade Cz-Si as a result of moderate temperature RTA treatments. A hypothesis is made about the mechanisms for this SiO₂ precipitation process.

Experimental

For the experiments, (100) double-sided polished p-type solar grade Cz-Si wafers cut from the top (higher perfection) and the bottom (lower perfection) parts of an ingot were used. Solar grade Si

material has a minority carrier lifetime of maximum 25 μs and a resistivity up to 10 Ω·cm, making it suitable for the fabrication of solar cells.¹¹ In addition, this material has a higher tolerance than microelectronic quality Si with respect to metallic contamination (up to 10¹³ cm⁻³).¹² The Si wafers under investigation had a diameter of 150 or 300 mm and a thickness in the range of 1–3 mm. The concentration of interstitial oxygen in the initial wafers was in the range of (8–10) × 10¹⁷ cm⁻³.

The wafers received two-step anneals, namely a furnace anneal at 800 °C during 10 h for the formation of SiO₂ precipitate nuclei, and subsequently a rapid thermal anneal (RTA) at 850 or 1050 °C in air for varying times. The transfer of samples from the furnace to the separate RTA chamber was done after that the samples had been cooled down to room temperature. The quick temperature raise during the rapid thermal anneals was achieved by heating the samples with a halogen lamp radiation system.

Fourier transform infrared (FTIR) spectroscopy was used to determine the concentrations of oxygen, both interstitial and precipitated in the SiO₂ phase. Float zone Si specimens with a low oxygen concentration (~2 × 10¹⁵ cm⁻³) were used as a reference. The intensities of the absorption bands of the valence oscillations of Si–O bonds (absorption maximum at about 1100 cm⁻¹) were measured. The measured optical density spectra were deconvoluted into elementary bands with a Gaussian shape. Standard parameters were used for the interstitial oxygen absorption band (maximum position at 1107 ± 1 cm⁻¹, full width at half-maximum 33 ± 1 cm⁻¹, respectively).¹³ A part of the absorption spectra in the low frequency range corresponds to the precipitated silicon oxide phase. It can be described by a number of Gaussian profiles with the parameters for the silicon-oxygen molecular complexes given in Table I.^{13–15}

The concentration of interstitial oxygen in the Si wafers was determined from the intensity of the O band using the coefficient $K = 3.03 \times 10^{17} \text{ cm}^{-3}$.¹³ The concentration of precipitated oxygen was estimated from the low frequency absorption band corresponding to the silicon oxide phase (sum of profiles P1, P2, and P3, see Table I).¹⁶

Details of the method for the calculation of the structural state of oxygen in the silicon oxide phase as well as the analysis of the uniqueness of the results of the mathematical treatment of the FTIR spectra were described in earlier publications.^{15,16}

Information about the type, the size, and the concentration of structural defects in Si wafers was obtained from the X-ray diffraction and electron microscopy investigations. In the former case, the widths at half-maximum of the diffraction reflection curves were measured and the X-ray diffuse scattering method was applied. The latter enables to reveal the presence and the type (vacancy or interstitial) of micro defects such as the inclusions of a new phase as well as point defect clusters that could not be resolved by electron

^z E-mail: andrey.sarikov@gmx.de

* Electrochemical Society Active Member.

** Electrochemical Society Fellow.

Table I. Characteristics of the elementary adsorption bands.

Band	Maximum, cm^{-1}	Width, cm^{-1}	Bonding angle of Si-O-Si	Basic structure component
O	1107 ± 1	33 ± 1	162°	Interstitial oxygen
P1	1085 ± 1	25 ± 1	142°	6-member rings of SiO_4 tetrahedra
P2	1060 ± 3	25 ± 2	132°	4-member rings of SiO_4 tetrahedra
P3	1035 ± 3	25 ± 3	126°	Molecular complexes $\text{Si-O}_2\text{-Si}_2$

microscopy due to the coherency with the silicon matrix, diffuse interface, and the small gradient of displacement fields. The diffraction reflection curves and the reciprocal space maps were measured using a high resolution X-ray diffractometer PANalytical X'Pert Pro MRD XL in the symmetrical 004 and asymmetrical 113 diffraction geometries under the irradiation from the $\text{CuK}\alpha_1$ source ($\lambda = 0.15406 \text{ nm}$). The curves of the distribution of the intensity of the diffuse scattering, $I(\mathbf{q})q^2$, were built in the direction parallel to the reciprocal lattice vector (q_z – cross-section) where \mathbf{q} is the vector from the reciprocal lattice site to the measurement point. The micro defects of the vacancy type are revealed in the curves by the maximum of $I(\mathbf{q})q^2$ at $q_z < 0$ and those of the interstitial type at $q_z > 0$, respectively. The characteristic defect sizes r_0 were determined from the maxima coordinates q_0 , i. e. $r_0 \propto \frac{1}{q_0}$. The micro defect concentrations are proportional to the values of $I(\mathbf{q})q^2$ in the maxima. More details on the procedure of X-ray diffraction and electron microscopy investigations can be found in Refs. 17 and 18.

The concentration of precipitated oxygen in the Si wafers prior to the thermal treatments was very low [$(\sim 2\text{--}5) \times 10^{16} \text{ cm}^{-3}$]. The oxygen precipitates had mostly a relaxed structure and consisted of 6-member rings of SiO_4 tetrahedra. Rapid thermal treatments (RTA) of the initial samples in air during 26 min had no noticeable influence on the concentrations of both interstitial and precipitated oxygen.

Furnace anneals (800°C , 10 h, Ar atmosphere) resulted in a decrease of the interstitial oxygen concentration in the investigated Si wafers. This effect was dependent on the specimen type. The concentration of interstitial oxygen was observed to decrease by ~ 45 and $\sim 15\%$ in the Si samples cut from the top and the bottom parts of the ingot, respectively. A strong increase in the concentration of precipitated oxygen was observed in the samples cut from the top part of the ingot, while only minor precipitation was detected for the Si samples cut from the bottom part of the ingot.

The temperature of the subsequent RTA treatment had a strong effect on the behaviour of the interstitial oxygen in the furnace annealed Si samples. It has been found that a RTA at 1050°C did not change the concentration of interstitial oxygen, while this concentration decreased significantly as a result of RTA treatments at 850°C . Figure 1 shows the concentration of interstitial oxygen in the RTA treated Si samples versus the RTA time. This figure clearly shows that the drop in the concentration of interstitial oxygen was more significant in the wafers cut from the top part of the ingot. The concentration of precipitated oxygen in the samples cut from the top and the bottom parts of the Si ingot were estimated to be $\sim 1.55 \times 10^{17} \text{ cm}^{-3}$ and $\sim 0.6 \times 10^{17} \text{ cm}^{-3}$, respectively, after a rapid thermal anneal for 37 min. In samples cut from the top part of the ingot, precipitates containing both 4-member rings of SiO_4 tetrahedra as well as molecular complexes of under-oxidised Si (such as SiO_2Si_2 and SiOSi_3) appeared together with 6-member rings of SiO_4 tetrahedra. In the Si samples cut from the bottom part of the ingot, the precipitates formed a weakly strained SiO_2 phase consisting of 6-member rings of SiO_4 tetrahedra (the low temperature α -cristobalite or quartz phase).^{19,20} The IR absorption spectra of the Si samples cut from the top and the bottom part of ingot showing the modifications of the oxygen state after different anneal stages are presented in Fig. 2. This figure also

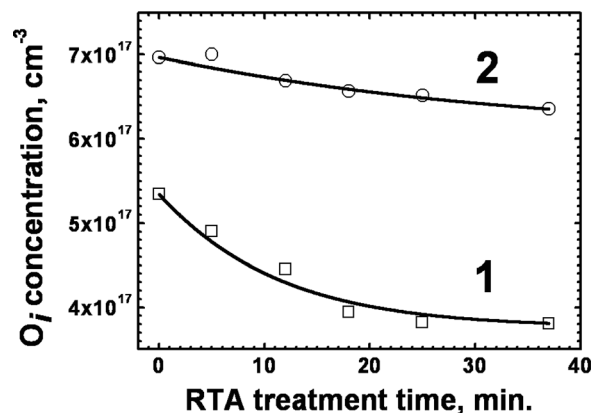


Figure 1. Experimental (dots) and calculated (lines) data of the interstitial oxygen concentration as functions of RTA treatment time at 850°C for Cz-Si wafers cut from the top (1) and the bottom (2) parts of the Si ingot.

shows the elementary peak positions obtained by the IR spectra deconvolution and the corresponding silicon-oxygen units composing the silicon oxide phase (see also Table I).

Figure 3 gives the distributions of the diffuse scattering in the q_z -cross-section for the Si samples cut from the top and the bottom parts of the ingot, respectively, before and after the thermal treatments. The ratios of the concentrations of built-in interstitial- and

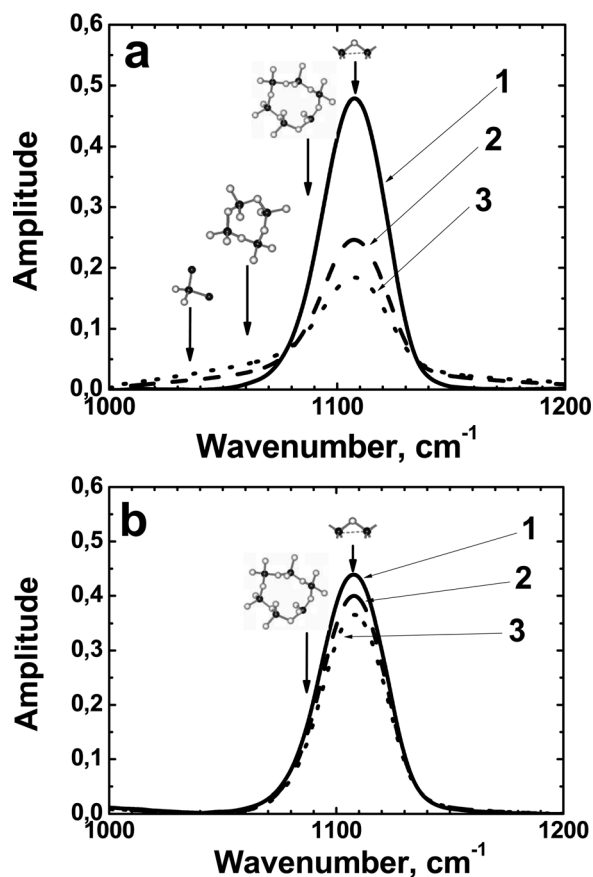


Figure 2. IR absorption spectra of the Si samples cut from the top (a) and the bottom (b) part of the ingot at different stages of the thermal treatment: 1—prior to anneal, 2—after 10 h furnace anneal at 800°C , and 3—after two step anneal (10 h at 800°C in furnace + 37 min RTA at 850°C). Arrows show the positions of elementary peaks corresponding to the interstitial oxygen and the silicon-oxygen units in the silicon oxide phase (see Table I). The respective atomic configurations are shown above the arrows.

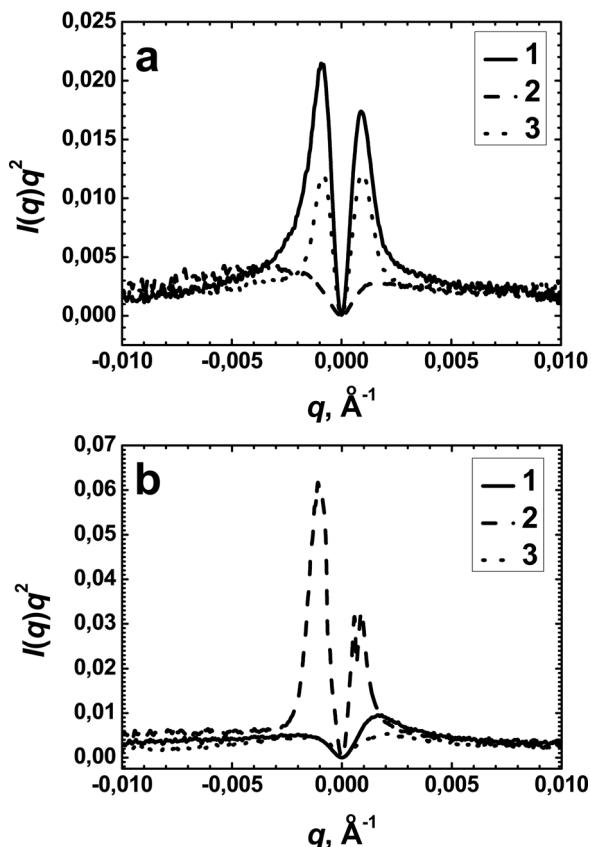


Figure 3. Distributions of the diffuse scattering in the q_z -cross-section for the Si samples cut from the top (a) and the bottom (b) parts of the ingot at different stages of the thermal treatment: 1—prior to anneal, 2—after 10 h furnace anneal at 800 °C, and 3—after two step anneal (10 h at 800 °C in furnace + 37 min RTA at 850 °C).

vacancy-type micro defects for the different treatment stages, obtained by the analysis of the data in Fig. 3, are shown in Fig. 4. Analysis of the evolution of the defect structures in the investigated Si wafers during the applied thermal treatments revealed some important features. The character of the distribution of the intensity of diffuse scattering $I(q)q^2$ in the initial Si samples demonstrated the presence of both vacancy ($q_z < 0$) and interstitial type ($q_z > 0$) micro defects. The contribution of the vacancy type micro defects was significantly higher in the Si wafers cut from the top part of the ingot

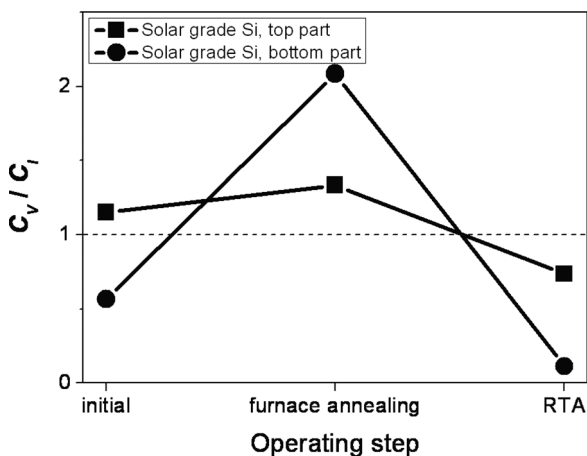


Figure 4. Dependence of the ratio of the concentrations of built-in interstitial- and vacancy-type micro defects on the RTA temperature for the Si wafers cut from the top and the bottom parts of the Si ingot.

and lower in the wafers cut from the bottom part, as compared to the contribution of the interstitial type micro defects (Fig. 4). Furnace anneals at 800 °C led to a drastic increase in the concentration of vacancy type micro defects in both types of wafers. This increase was much stronger in the Si wafers cut from the bottom part of the Si ingot so that the relative contribution of vacancy type micro defects in these wafers became almost twice as large as in the wafers cut from the top part of the Si ingot. A disappearance of fine micro defects was observed in the Si samples cut from the top part of the ingot, most likely caused by the defect coalescence at elevated temperatures.

RTA treatments led to a significant change of the relative contributions of the different types of micro defects. Interstitial type micro defects became prevalent in both types of Si wafers. This effect was more significant for the Si wafers cut from the bottom part of the ingot.

The modifications of the oxygen state as well as the nature of the defects in the Si wafers after RTA treatments at 850 °C were stable in time. The IR spectra of the investigated samples did not change after storage of Si wafers during half a year in air.

Finally, some Si specimens annealed in a furnace at 800 °C during 10 h as well as specimens after two-step treatment (furnace anneal at 800 °C plus RTA in air) were subjected to an additional furnace anneal at 1050 °C in an Ar atmosphere for up to 2 h. The behaviour of all the samples was identical. The concentration of interstitial oxygen decreased and the concentration of oxygen precipitated in the SiO₂ phase increased as a result of such a treatment. The efficiency of this process did almost not depend on the sample treatment before the high temperature anneals.

Precipitation Model

The kinetics of the oxygen precipitation during the RTA treatments at 850 °C can be described in the framework of the mathematical model proposed earlier.¹⁰ In a first approximation, this model states that prior to the RTA treatments, equal-size spherical shape SiO₂ precipitates with radii R_0 and concentration N_p are formed by a furnace anneal at 800 °C. The model uses a diffusion limited supply of oxygen for the growing precipitates. The equations describing the evolution of the concentrations of mobile interstitial oxygen, C_i , and precipitated oxygen, C_p , as well as the average precipitate radius, R , are given by (Ref. 21)

$$\frac{dC_i}{dt} = -\frac{dC_p}{dt} = -4\pi DRN_p \left[C_i - C_{if}^0 \exp\left(\frac{2\sigma\Omega}{Rk_B T}\right) \right] \quad [1]$$

$$\frac{dR}{dt} = \frac{D\Omega}{R} \left[C_i - C_{if}^0 \exp\left(\frac{2\sigma\Omega}{Rk_B T}\right) \right] \quad [2]$$

Here, D is the diffusion coefficient of oxygen in bulk Si, $\Omega = 2.25 \times 10^{-29} \text{ m}^3$ is the volume per oxygen atom in the silicon oxide phase,²¹ C_{if}^0 is the equilibrium concentration of interstitial oxygen for a flat SiO₂/Si interface, $\sigma = 0.43 \text{ J/m}^2$ is the specific energy of the interface of the SiO₂ precipitate with the Si matrix,²² k_B is the Boltzmann constant, and T is the RTA temperature, respectively. The exponential term in the right hand sides of Eqs. 1 and 2 takes into account the dependence of the equilibrium concentration of interstitial oxygen in the vicinity of precipitates on the precipitate surface curvature (Gibbs-Thompson effect).

The initial concentrations of interstitial oxygen in the Si wafers cut from the top and the bottom parts of the ingot corresponded to the values obtained after the furnace anneal at 800 °C and amounted to $5.34 \times 10^{17} \text{ cm}^{-3}$ and $6.97 \times 10^{17} \text{ cm}^{-3}$, respectively. The initial precipitate radius R_0 and the precipitate concentration N_p are functions of the total concentration of precipitated oxygen prior to the RTA treatments, C_p^0

$$\frac{4\pi R_0^3}{3\Omega} N_p = C_p^0 \quad [3]$$

The values of C_p^0 were calculated as the differences between the interstitial oxygen concentrations prior to and after the furnace anneals and were equal to $4.2 \times 10^{17} \text{ cm}^{-3}$ and $1.4 \times 10^{17} \text{ cm}^{-3}$ for the Si wafers cut from the top and the bottom parts of the ingot, respectively. Therefore, by determining either of the parameters R_0 and N_p , one may calculate the other parameter. In our case, the initial precipitate radius was treated as an unknown parameter and was fitted to achieve the best agreement between the experimental data and the simulation results.

The equilibrium concentration of interstitial oxygen at the flat Si/SiO₂ interface, C_{ij}^0 , was treated here as another free parameter that qualitatively reflects the defect state in the sample and has therefore to be determined using the experimental data.

Results

Figure 1 shows the dependences of the calculated interstitial oxygen concentration on the time of the RTA treatment at 850 °C for Si wafers cut from the top and the bottom parts of the ingot, obtained by fitting the experimental data. The fitting was done by minimization of the least-square deviation of the calculated curves from the experimental points. The calculations demonstrate that the concentration of interstitial oxygen in the Si wafers decreases with the time of the RTA treatment and tends to saturate. The saturation in the Si wafers cut from the bottom part of the ingot occurs at a higher interstitial oxygen concentration than in the wafers cut from the top part of the ingot. Both concentrations exceed the saturation level of interstitial oxygen of about $1.32 \times 10^{16} \text{ cm}^{-3}$ at 850 °C reported in the literature.²²

Fitting of simulation results to the experimental data on the decrease of the interstitial oxygen concentration in Si wafers subjected to RTA anneals demonstrated that the standard values of the diffusivity and the solubility limit of oxygen in crystalline Si could not be used. An adequate description of the experimental data required to treat these quantities as parameters. The fitting parameters used in the theoretical model of oxygen precipitation during the RTA treatments are shown in Table II, together with their ratios to the standard values. The confidence level of the fitting parameters is high since small changes in them lead to large modifications of the calculated curves and their deviations from the experimental points. One can see that the precipitate radii prior to the RTA treatments do not differ much for the wafers cut from the top and the bottom parts of the ingot. This means a more efficient precipitate nucleation process in Si wafers cut from the top part of the ingot, in view of the higher concentration of precipitated oxygen in these samples as a result of the furnace pre-anneals. The values of oxygen diffusivities leading to the observed precipitation kinetics are about three orders of magnitude higher than the reported diffusivity value of interstitial oxygen in Si (Ref. 22) and differ by 2 times for the Si wafers cut from the top and the bottom part of the ingot. The simulated values of the equilibrium concentration of interstitial oxygen exceed the reported solubility limit by about 26.6 and 45 times for the Si wafers cut from the top and the bottom parts of the ingot, respectively. This hints to new phenomena involved in the oxygen precipitation process during the rapid thermal anneals compared to the case of traditional furnace anneals. These phenomena are considered in detail in the next section.

Table II. Fitting parameters of the oxygen precipitation model in Cz-Si during RTA treatments.

	$R_0(\text{nm})$	$D(\text{cm}^2 \text{ s}^{-1})$	D/D_i^a	C_{ij}^0/C_i^{eqb}
Bottom part of ingot	40.0	8.53×10^{-14}	1563.06	45.0
Top part of ingot	32.3	4.33×10^{-14}	793.44	26.6

^a $D_i = 0.13 \times \exp(-2.53/k_B T) \text{ cm}^2/\text{s}$ is the tabular value of the diffusivity of interstitial oxygen in Si (Ref. 20).

^b $C_i^{eq} = 9 \times 10^{22} \times \exp(-1.52/k_B T) \text{ cm}^{-3}$ is the tabular value of the solubility limit of interstitial oxygen in Si (Ref. 20).

Discussion

Oxygen solubility.—High temperature RTA treatments of Si wafers in a nitrogen atmosphere are known to introduce excess vacancies.^{6,9} Alternatively, treatments in an oxygen atmosphere introduce Si self-interstitials.¹ Therefore, the rapid thermal anneals of Si wafers in air are expected to introduce defects of both types in different quantities that depend not only on the relative concentrations of oxygen and nitrogen in the air but also on the defect generation rates. In addition, noticeable concentrations of both vacancy and interstitial type micro defects in Si wafers prior to the rapid thermal anneal are detected by X-ray diffraction investigations. All the defects, both those already present in the Si wafers and those generated during the rapid thermal anneals, should participate in the oxygen precipitation process modifying both the equilibrium concentration and the diffusivity of oxygen in Si during the RTA treatment at 850 °C.

The increase of the equilibrium concentration of oxygen during the RTA treatments can be understood in the framework of the nucleation model proposed by Vanhellemont and Claeys.⁵ In their model, the change of the Gibbs free energy associated with the formation of a spherical SiO₂ precipitate with j oxygen atoms (having radius R_j) is given by the following expression

$$W_j = -jk_B T \ln \left[\frac{C_i}{C_i^{eq}} \left(\frac{V}{V_{eq}} \right)^\beta \left(\frac{I}{I_{eq}} \right)^{-\gamma} \right] + (36\pi\Omega^2)^{1/3} \sigma_j^{2/3} \quad [4]$$

where C_i^{eq} is the standard value of oxygen solubility in crystalline Si, V and V_{eq} are the concentration and the solubility limit of vacancies in crystalline Si, I and I_{eq} are the concentration and the solubility limit of Si self-interstitials in crystalline Si, and β and γ are the numbers of vacancies and Si self-interstitials absorbed and emitted per one oxygen atom incorporated into the precipitate, respectively. In expression 4, the stress contribution in the Gibbs free energy associated with the formation of a silicon oxide precipitate with radius R_j is neglected. It is assumed here that the stress is fully released upon the vacancy absorption and/or Si self-interstitial emission during the precipitate growth. This assumption is plausible especially for the Si wafers cut from the bottom part of the ingot in view of the experimental observation of the formation of unstrained SiO₂ precipitates with 6-member rings of SiO₄ tetrahedra.

The concentration of interstitial oxygen in Si can change as a result of the growth and dissolution of SiO₂ precipitates. The kinetics of this process in the case of large precipitates, i. e. when addition or subtraction of one oxygen atom has a negligible influence on the precipitate radius, is described by the following equation:

$$\frac{dC_i}{dt} = -(k_j^+ C_i - k_j^-) N_p \quad [5]$$

where $k_j^+ = 4\pi DR_j$ and k_j^- are the kinetic coefficients determining the rates of diffusion limited precipitate growth and dissolution, respectively. The relation between the kinetic coefficients k_j^+ and k_j^- in the classical nucleation theory is expressed as follows²³:

$$k_j^- = k_j^+ C_i \exp\left(\frac{\delta W(R_j)}{k_B T}\right) \quad [6]$$

where $\delta W(R_j)$ is the change of the Gibbs free energy upon addition of one oxygen atom to a precipitate of radius R_j . Using formula 4, this expression acquires the following form:

$$\delta W(R_j) = -k_B T \ln \left[\frac{C_i}{C_i^{eq}} \left(\frac{V}{V_{eq}} \right)^\beta \left(\frac{I}{I_{eq}} \right)^{-\gamma} \right] + \frac{2\sigma\Omega}{R_j} \quad [7]$$

It is taken into account here that $\frac{4\pi R_j^3}{3\Omega} = j$ and $4\pi\sigma(R_{j+1}^2 - R_j^2) \approx 8\pi\sigma R_j \frac{dR_j}{dj} = \frac{2\sigma\Omega}{R_j}$, respectively.

Combining expressions 5–7, the following equation is obtained for the kinetics of the change of the concentration of interstitial oxygen during the RTA treatments

$$\frac{dC_i}{dt} = -4\pi DR_j N_p \left[C_i - C_i^{eq} \left(\frac{V}{V_{eq}} \right)^{-\beta} \left(\frac{I}{I_{eq}} \right)^\gamma \exp \left(\frac{2\sigma\Omega}{R_j k_B T} \right) \right] \quad [8]$$

Comparing Eqs. 1 and 8, the equilibrium concentration of oxygen in Si is determined in the following way:

$$C_{if}^0 = C_i^{eq} \left(\frac{V}{V_{eq}} \right)^{-\beta} \left(\frac{I}{I_{eq}} \right)^\gamma \quad [9]$$

It follows from expression 9 that the equilibrium concentration of oxygen in the presence of excess point defects is to a large extent determined by the point defect supersaturation. Excess vacancies promote oxygen precipitation and, hence, the decrease of the equilibrium concentration of interstitial oxygen in Si. On the other hand, the presence of excess Si self-interstitials promotes the precipitate dissolution and the increase of the oxygen concentration in equilibrium with the precipitated phase.

The absorption of vacancies and the emission of Si self-interstitials during the oxygen precipitation lead to the release of strain caused by the different volumes of Si and SiO₂. It is believed that the release of strain associated with the incorporation of one oxygen atom in the precipitate requires absorption of ~0.6 vacancies or, alternatively, emission of one half Si self-interstitial,^{6,24} so that $\beta=0.6$ and $\gamma=0.5$, respectively. Using these numbers, one may calculate the required supersaturation with vacancies and Si self-interstitials that are necessary to increase the equilibrium concentration of interstitial oxygen by the factors shown in Table II. Figure 5 shows the interrelations of the supersaturation with vacancies and Si self-interstitials to achieve the values of $\left(\frac{V}{V_{eq}} \right)^{-\beta} \left(\frac{I}{I_{eq}} \right)^\gamma$ equal to 26.6 and 45 for the Si wafers cut from the top and the bottom parts of the ingot, respectively. It can be seen that the values of supersaturation with interstitial Si atoms required to provide the calculated equilibrium concentrations of interstitial oxygen are by about 3 to 4 orders of magnitude larger than those for the vacancies. This is not quite surprising and unrealistic, however, in view of the 4 orders of magnitude smaller value of the equilibrium concentration of Si self-interstitials compared to that of vacancies at the RTA temperature (1.45×10^{10} vs. 1.42×10^{14} cm⁻³ at 850°C, respectively).²⁵ As one may see from Fig. 5, the relative numbers of Si self-interstitials that are in action during the RTA process should be higher in the case of Si wafers cut from the bottom part of the ingot. This is supported by

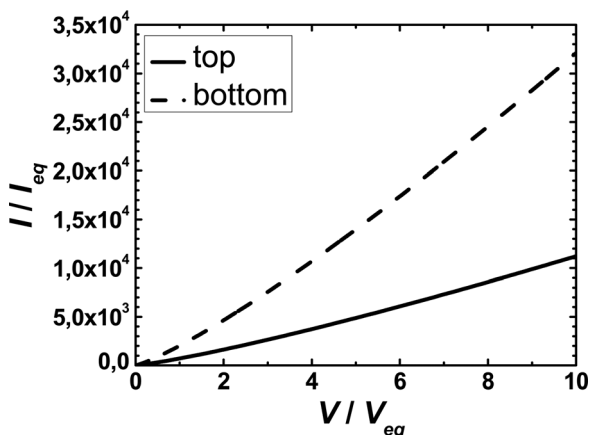


Figure 5. The interrelations of the supersaturation with vacancies and Si self-interstitials to achieve the values of $\left(\frac{V}{V_{eq}} \right)^{-\beta} \left(\frac{I}{I_{eq}} \right)^\gamma$ equal to 26.6 and 45 for the Si wafers cut from the top and the bottom parts of the Si ingot, respectively.

the data of Fig. 4, where the much higher impact of the interstitial type defects in these wafers compared to the wafers cut from the top part of the Si ingot is demonstrated.

Oxygen diffusivity.— It is reasonable to suppose that the increase of the effective diffusivity of oxygen in the case of RTA treatments at 850°C is mainly related to the excess point defects generated during the treatments. Due to the air atmosphere in which the Si wafers are processed, one should expect the generation of both excess vacancies and Si self-interstitials in the bulk Si. Complexes of oxygen atoms with point defects have been proposed in the literature as candidates for fast diffusers in Si.^{26,27} The oversaturation with point defects increases the concentration of oxygen atom-point defect complexes and therefore increases their contribution to the oxygen diffusion rate.

The mechanism for the increase of the effective oxygen diffusivity by considering complexes consisting of an oxygen atom with a point defect denoted as A (vacancy or Si self-interstitial, i. e. A = V or I, respectively) has been analyzed. The reaction between interstitial oxygen and the point defect A can be described in the following way:



where the OA complex is mobile and its diffusivity far exceeds the diffusivity of interstitial oxygen. The concentration of OA complexes depends on the concentrations of both interstitial oxygen atoms and point defects A as well as on the solubility concentrations of all three species in reaction 10. From the mass action law

$$\frac{C_i \times C_A}{C_{OA}} = \frac{C_i^{eq} \times C_A^{eq}}{C_{OA}^{eq}} \quad [11]$$

and therefore

$$C_{OA} = \frac{C_i \times C_A}{C_i^{eq} \times C_A^{eq}} C_{OA}^{eq} \quad [12]$$

In formulas 11 and 12, C_A and C_{OA} are the concentrations of species A and OA, respectively, and C_A^{eq} and C_{OA}^{eq} are their solubilities, respectively.

The total flow of oxygen J as a result of the diffusion of both interstitial oxygen atoms and OA complexes is obtained from Fick's law

$$J = -D \frac{\partial C_i}{\partial x} = -D_i \frac{\partial C_i}{\partial x} - D_{OA} \frac{\partial C_{OA}}{\partial x} \quad [13]$$

Assuming a homogeneous concentration of point defects throughout the whole Si wafer thickness (the diffusivities of point defects at 850°C exceed the diffusivity of oxygen atoms by several orders of magnitude), formula 13 can be rewritten as

$$J = - \left(D_i + D_{OA} \frac{C_{OA}^{eq} \times C_A}{C_i^{eq} \times C_A^{eq}} \right) \frac{\partial C_i}{\partial x} \quad [14]$$

The effective oxygen diffusivity can therefore be expressed in the following form:

$$D = D_i + D_{OA} \frac{C_{OA}^{eq} \times C_A}{C_i^{eq} \times C_A^{eq}} \quad [15]$$

Formula 15 shows that the effective oxygen diffusivity is directly proportional to the supersaturation with point defects A as well as to the diffusivity of the OA complexes. From formula 15, one may determine $D_{OA} C_{OA}^{eq}$ to achieve the values of D from Table II as a function of supersaturation with point defects. The respective results are presented in Fig. 6. One can see that the values of $D_{OA} C_{OA}^{eq}$ are inversely proportional to the supersaturation of point defects A and

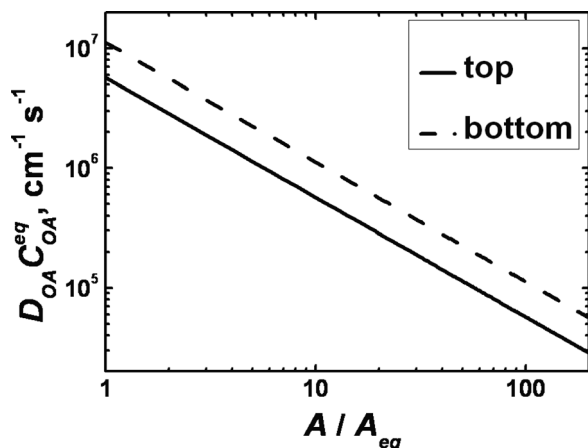


Figure 6. Values of $D_{OA}C_{OA}^{eq}$ as functions of the supersaturation with point defects to achieve the increase of effective oxygen diffusivity by 793.44 and 1563.06 times for the Si wafers cut from the top and the bottom parts of the Si ingot, respectively.

lie in the range $\sim 10^7\text{--}10^5\text{ cm}^{-1}\text{ s}^{-1}$ for a supersaturation in the range of 1–200, respectively.

The values of $D_{OA}C_{OA}^{eq}$ can be compared to the respective value for oxygen. The product of the diffusivity of interstitial oxygen in bulk Si with its solubility is equal to $\sim 7.2 \times 10^3\text{ cm}^{-1}\text{ s}^{-1}$ at 850 °C. This means that for comparable solubilities of interstitial oxygen and OA complexes, the diffusivity of the oxygen-point defect complex should exceed that of interstitial oxygen by up to 3 orders of magnitude and become higher for smaller OA solubilities. Such values are, however, not unreasonable. For instance, the reported values of the pre-factor and the activation energy of the diffusion of VO complexes in Si are $6\text{ cm}^2/\text{s}$ and 1.8 eV ,²⁶ respectively, which gives a value for the VO diffusivity of $\sim 4.83 \times 10^{-8}\text{ cm}^2/\text{s}$ at 850 °C. This value is about 6 orders of magnitude higher than the diffusivity of interstitial oxygen at this temperature. The authors are not aware of published data for OI complexes. It is reported that $D_{VO} > D_{OI}$,²⁸ which means that a higher Si self-interstitials supersaturation is required assuming their participation in the oxygen diffusion process to achieve the effective oxygen diffusivity values reported in Table II. However, the supersaturation with Si self-interstitials is achieved easier than that for the vacancies in view of the much smaller solubility at 850 °C. So that, complexes of oxygen atoms with both vacancies and Si self-interstitials cannot be excluded as cause for the enhanced oxygen diffusion during the rapid thermal anneals of Cz-Si wafers at 850 °C.

It should be noted that other fast diffusing oxygen related species such as oxygen-hydrogen or oxygen-carbon pairs,²⁰ quasi free oxygen atoms and oxygen dimers²⁹ were proposed to account for the enhanced diffusivity of oxygen in Si. However, these mechanisms are hardly dependent on the presence or absence of excess point defects and thus there should be no difference between the oxygen precipitation kinetics due to furnace or rapid thermal anneals. The observed difference in this work still implies the participation of excess point defects generated during the RTA treatment at 850 °C in the precipitation of oxygen.

Conclusion

In this work, the mechanisms leading to the experimentally observed peculiarities of the kinetics of oxygen precipitation in Si wafers subjected to rapid thermal anneals are analysed. A model for oxygen precipitation is proposed that takes into account the remarkable increase of the concentration as well as the diffusivity of oxygen in Si compared to the equilibrium values reported in the literature; namely the influence of excess point defects on both the equilibrium oxygen concentration and its diffusivity in Si is analysed. The

observed increase of the equilibrium concentration of oxygen by more than an order of magnitude (~ 30 and ~ 45 times in our case for the Si wafers cut from the top and the bottom parts of the Si ingot, respectively) is consistent with the increase of the energetic barrier for the precipitate formation as a result of the interaction with excess point defects generated during the RTA treatments. The increase of the effective diffusivity of oxygen atoms by up to 3 orders of magnitude (~ 800 and ~ 1500 times for the Si wafers cut from the top and the bottom parts of the Si ingot, respectively) is caused by the formation of fast diffusing complexes of oxygen atoms with point defects. The difference in the precipitation of interstitial oxygen in the Si wafers cut from the bottom and the top parts of the ingot results from the different point defect oversaturation during the RTA treatment probably related to the micro defect state and its influence on the point defect behavior.

Acknowledgments

This work has been carried in the framework of the project $\Phi 28.7/051$ “Development of the scientific principles of the technology for the formation of dislocation free large diameter Si single crystals using the Czochralski method and the thermal treatments that control the state of oxygen atoms in the crystal lattice” of the Ministry of Education and Science of Ukraine as well as the project 3.3–10 “Development and implementation of the technology for the formation of stress free homogeneous Si ingots” of the Research and Development Programme “Creation of Chemical and Technology Branch of the Production of Pure Silicon Material” (No. 1173).

References

1. M. Akatsuka, M. Okui, N. Morimoto, and K. Sueoka, *Jpn. J. Appl. Phys. Part 1*, **40**, 3055 (2001).
2. H. Wang, X. Ma, J. Xu, X. Yu, and D. Yang, *Semicond. Sci. Technol.*, **19**, 715 (2004).
3. G. A. Hawkins and J. P. Lawine, *J. Appl. Phys.*, **65**, 3644 (1989).
4. R. Falster, V. V. Voronkov, and F. Quast, *Phys. Status Solidi B*, **222**, 219 (2000).
5. J. Vanhellemont and C. Claeys, *J. Appl. Phys.*, **62**, 3960 (1987).
6. R. Falster, M. Pagani, D. Gambaro, M. Cornara, M. Olmo, G. Ferrero, P. Pichler, and M. Jacob, *Solid State Phenom.*, 57–58, 129 (1997).
7. M. Pagani, R. J. Falster, G. R. Fisher, G. C. Ferrero, and M. Olmo, *Appl. Phys. Lett.*, **70**, 1572 (1997).
8. X. Ma, L. Lin, D. Tian, L. Fu, and D. Yang, *J. Phys.: Condens. Matter*, **16**, 3563 (2004).
9. K. Tempelhoff and M. Van Sung, *Phys. Status Solidi*, **72**, 617 (1982).
10. V. Litovchenko, I. Lisovskiy, M. Voitovich, A. Sarikov, S. Zlobin, V. Kladko, and V. Machulin, *Solid State Phenom.*, **156–158**, 279 (2010).
11. W. Koch, A. L. Endroes, D. Franke, C. Haepler, J. P. Kalejs, and H. J. Moeller, in *Handbook of Photovoltaic Science and Engineering*, A. Luque and S. Hegedus, Editors, pp. 205–254, John Wiley & Sons, Chichester, 2003.
12. Ye. Ya, Shvets and Yu, V. Golovko, Metallurgy, In press [in Russian].
13. B. Pajot, H. J. Stein, B. Cales, and C. Naud, *J. Electrochem. Soc.*, **132**, 3034 (1985).
14. K. Tempelhoff, F. Spiegelberg, R. Gleichmann, and D. Wruck, *Phys. Status Solidi A*, **56**, 213 (1979).
15. I. P. Lisovskii, V. G. Litovchenko, V. B. Lozinskii, and G. I. Steblivskii, *Thin Solid Films*, 213, 164 (1992).
16. I. P. Lisovskii, V. G. Litovchenko, V. B. Lozinskii, S. I. Frolov, H. Flietner, W. Fussel, and E. G. Schmidt, *J. Non-Cryst. Solids*, **187**, 91 (1995).
17. V. T. Bublik and K. D. Shcherbachev, *Crystallogr. Rep.*, **42**, 286 (1997).
18. V. P. Kladko, L. I. Datsenko, J. Bak-Misiuk, S. I. Olikhovskii, V. F. Machulin, I. V. Prokopenko, V. B. Molodkin, and Z. V. Maksimenko, *J. Phys. D: Appl. Phys.*, **34**, A87 (2001).
19. A. G. Revesz, *Phys. Status Solidi*, **57**, 235 (1980).
20. V. G. Litovchenko and A. P. Gorban, *Principles of Physics of Microelectronic MIS Systems*, pp. 60–80, Naukova Dumka, Kiev (1978) [in Russian].
21. V. G. Litovchenko, I. P. Lisovskiy, V. P. Kladko, S. O. Zlobin, M. V. Murav'ska, A. A. Efremov, and M. V. Slobodyan, *Ukr. J. Phys.*, **5**, 958 (2007).
22. A. Borghesi, B. Pivac, A. Sassella, and A. Stella, *J. Appl. Phys.*, **77**, 4169 (1995).
23. J. W. Christian, *The Theory of Transformations in Metals and Alloys*, 2nd ed., Pergamon Press, Oxford, (1979).
24. F. K. LeGoues, R. Rosenberg, T. Nguyen, F. Himpsei, and S. Meyerson, *J. Appl. Phys.*, **65**, 1724 (1989).
25. C. del Cañizo and A. Luque, *J. Electrochem. Soc.*, **147**, 2685 (2000).
26. P. Pichler, *Intrinsic Point Defects, Impurities, and Their Diffusion in Silicon*, Springer-Verlag, Wien (2004).
27. A. Ourmazd, W. Schröter, and A. Bourret, *J. Appl. Phys.*, **56**, 1670 (1984).
28. D. Heck, R. E. Tressler, and J. Monkowski, *J. Appl. Phys.*, **54**, 5739 (1983).
29. L. I. Murin, T. Hallberg, V. P. Markevich, and J. L. Lindström, *Phys. Rev. Lett.*, **80**, 93 (1998).